TABLE I. Summary of systematic errors affecting the K^0-K^+ mass difference.

Origin of error	Uncertainty	Effect on ΔM
Liquid density	0.0002 g/cm^3	0.07 MeV
Average magnetic field	20 G	0.08 MeV
K^+ mass	0.11 MeV	0.04 MeV

K^+ mass was varied, the magnetic field was also re-calculated, since the latter was determined by measurements of $K^+ \to 3\pi$ decays. The errors introduced in ΔM from the one-standard-deviation uncertainties in these quantities are presented in Table I.

Finally, combining the statistical and systematic errors as independent quantities, we obtained as our best estimate of the K^0-K^+ mass difference

$$M_{K^0} - M_{K^+} = 3.95 \pm 0.21 \text{ MeV}.$$

A value of 5.4 ± 1.1 MeV for the (K^0-K^+) mass has been obtained previously by Crawford *et al.*[1] Measure-

ments of the $\bar{K}^0$-K^- mass difference are 3.9 ± 0.6 MeV by Rosenfeld *et al.*,[2] 3.90 ± 0.25 MeV by Burnstein *et al.*,[3] 3.71 ± 0.35 MeV by Kim *et al.*,[4] and 4.18 ± 0.18 MeV by Engelmann *et al.*[5] Our value of ΔM is in agreement with these other measurements.

Using all the above data, and the fact that $M_{K^0} - M_{\bar{K}^0} \leq 10^{-14}$ MeV,[8] we obtained $M_{K^+} - M_{K^-} = 0.02 \pm 0.24$ MeV.[9]

ACKNOWLEDGMENTS

We would like to thank Dr. N. P. Samios for his generous support. We are grateful to Mrs. V. Austen, who has ably organized the computer runs. We also acknowledge the careful work of our scanning and measuring staffs.

[8] M. L. Good, Proceedings of the Argonne International Conference on Weak Interactions, 1965, Argonne National Laboratory Report No. ANL-7130, p. 215 (unpublished).
[9] This can be compared to the result in the compilation of Ref. 7; $M_{K^+} - M_{K^-} = 0.1 \pm 0.4$ MeV.

Quasifree Nucleon-Nucleon Bremsstrahlung at 197 MeV*

P. F. M. Koehler,† K. W. Rothe,‡ and E. H. Thorndike

Department of Physics and Astronomy, University of Rochester, Rochester, New York

(Received 5 July 1967)

Quasifree nucleon-nucleon bremsstrahlung processes have been studied at 197 MeV by bombarding a target of liquid deuterium with a 90% polarized proton beam. A γ detector gave the directions of photons of energy $E_\gamma \geq 40$ MeV; spark chambers triggered by large-area counters were used to determine the direction(s) and range(s) of the energetic charged particle(s) which emerged in coincidence with a γ ray. Samples of events from three final states were extracted: (1) $p+d \to n_s+p+p+\gamma$; (2) $p+d \to p_s+d+\gamma$; (3) $p+d \to p+d+\gamma$. Events of type (1) exhibited angular distributions and a γ spectrum in agreement with free $pp\gamma$ results, while the cross sections were reduced by a factor of 0.50 ± 0.10. Differential cross sections for reaction (2) were found to be reduced by a factor of 0.75 ± 0.15 from the values predicted for the free capture reaction; the γ-ray asymmetries were in good agreement with predictions from deuteron photodisintegration; the branching ratio for the production of the n-p system in the slightly unbound final state to that in the bound $^3S_1$ final state was found to be 0.22 ± 0.04. The cross section for reaction (3) was small, and its study was strongly limited by the detection thresholds of the spark chambers. Events from the reaction $p+d \to p_s+n+p+\gamma$ could not be identified with our apparatus, but they were the only other contributors to the coincidence rates between a γ ray and a single charged particle. By subtracting the measured contributions from reactions (1)–(3) from them, we obtained differential cross sections for quasifree n-p bremsstrahlung at three angles. We deduced cross sections for free $np\gamma$ from them and found $\sigma_{np\gamma} = 35 \pm 12$ μb. This result implies a ratio $\sigma_{np\gamma}/\sigma_{pp\gamma} = 50 \pm 20$.

I. INTRODUCTION

SEVERAL electromagnetic interactions provide information about the nucleon-nucleon interaction off mass shell. Among them, the process of nucleon-nucleon

bremsstrahlung $(N+N \to N+N+\gamma)$ is well suited to test the various existing theoretical pictures of the N-N interaction, and to provide input information for nuclear-structure calculations. Recent improvements in accelerator performance and particle detection have made possible the experimental study of these bremsstrahlung processes, whose cross sections are typically

three orders of magnitude lower than the elastic cross sections. Proton-proton bremsstrahlung (hereafter $pp\gamma$) experiments[1–5] have now been performed at several laboratories over a wide range of energies; these measurements, in turn, have revitalized the theoretical interest[6–11] in this process. Theory and experiment have now converged to fair agreement, but the conclusions which can be drawn have fallen short of some early expectations.

In order to achieve a more complete understanding of the N-N interaction off mass shell, the process of neutron-proton bremsstrahlung (hereafter $np\gamma$) must be considered as well. Early calculations of the $np\gamma$ cross section by Ashkin and Marshak[6] and by Simon[12] indicated that it was almost one order of magnitude larger than the $pp\gamma$ cross section. These predictions led to the first experimental efforts to measure nucleon-nucleon bremsstrahlung: Protons were scattered from complex nuclei, and γ rays of higher energy than expected from nuclear de-excitation ($E_\gamma > 20$ MeV) were detected. At incident proton energies below the threshold for π^0 production, the γ radiation produced could be ascribed to $NN\gamma$, and the predicted ratio[6] $\sigma_{np\gamma}/\sigma_{pp\gamma} \sim 10$ suggested that nearly all of it was due to $np\gamma$ inside the nucleus. Such experiments were performed by Wilson,[13] Cohen et al.,[14] and Edgington and Rose.[15] However, the extraction of quantitative information about free $np\gamma$ from such measurements is both difficult and dubious, as shown by Beckham,[16] who contributed the most applicable theoretical treatment of bremsstrahlung from proton-nucleus collisions and applied it to the measurements of Cohen et al.[14] He found that the exclusion principle caused a strong reduction of the radiation production, especially for photons of high energy, and that the choice of the momentum distribution for the target nucleons critically affected the calculated cross sections.

Unfortunately, a free-$np\gamma$ measurement depends on the availability of a neutron beam of well-defined energy

and high intensity. Since no such beam is yet available, one must turn to deuterium as a target of "almost-free" neutrons, an alternative which was recognized long ago and employed successfully in elastic N-N scattering.[17] It was first applied to a bremsstrahlung experiment by Edgington and Rose,[18] who measured the γ radiation resulting from the bombardment of D_2O and H_2O targets by 140-MeV protons, and extracted $np\gamma$ cross sections by subtraction. The large amount of background radiation resulting from the presence of the oxygen prevented them from identifying the radiative channels through the detection of charged particles in coincidence with the γ ray.

The present experiment avoided this limitation by using a liquid-deuterium target. By detecting the charged particles emerging in coincidence with the γ ray, we were able to identify most of the final states which contributed to the radiation production. The interpretation of our results in terms of the underlying $NN\gamma$ processes was done with the help of an impulse-approximation model as described in Sec. II of this paper. After a sketch of the experimental methods employed in this experiment in Sec. III, the data reduction is outlined in Sec. IV. The results are presented in Sec. V and discussed in the light of previous measurements in Sec. VI.

II. THEORETICAL MODEL

The statement that deuterium provides a target of "almost-free" neutrons and protons summarizes the spirit of the impulse approximation.[19] It is based on the fact that the deuteron is a very loosely bound structure in which the nucleons will act like independent particles a large part of the time. If the wavelength of an incident particle is less than the average spacing between the target nucleons, we can assume that it interacts with only one of them, while the other one will remain a spectator. If the struck nucleon gains sufficient momentum to be detected, we can determine the type of scattering which took place. The main difference between a quasifree N-N interaction in deuterium and a free one is the fact that the target nucleon in deuterium is not at rest. Its momentum distribution can be obtained from the known deuteron wave function. Furthermore, we expect a reduction of the quasifree cross sections below the free ones due to Glauber shielding,[20] and to final-state interactions which may distort the kinematics or lead to binding of the particles.

In the present experiment the incident protons had an energy of 197 MeV, and their wavelength was thus sufficiently small to permit the application of the impulse approximation. We say, then, that the incident proton will interact with only one of the two target nucleons to produce bremsstrahlung. Neglecting all

[1] B. Gottschalk, W. J. Shlaer, and K. H. Wang, Phys. Letters **16**, 294 (1965); Nucl. Phys. **75**, 549 (1966).

[2] R. E. Warner, Can. J. Phys. **44**, 1225 (1966).

[3] I. Slaus, J. W. Verba, J. R. Richardson, R. F. Carlson, W. T. H. van Oers, and L. S. August, Phys. Rev. Letters **17**, 536 (1966).

[4] K. W. Rothe, P. F. M. Koehler, and E. H. Thorndike, Phys. Rev. **157**, 1247 (1967).

[5] M. L. Halbert, D. L. Mason, and C. L. Northcliffe, Rev. Mod. Phys. **39**, 716 (1967).

[6] J. Ashkin and R. E. Marshak, Phys. Rev. **76**, 58 (1949); **76**, 989 (1949).

[7] C. Dullemond and J. J. de Swart, Physica **26**, 664 (1960).

[8] M. I. Sobel and A. H. Cromer, Phys. Rev. **132**, 2698 (1963).

[9] I. Duck and W. A. Pearce, Phys. Letters **21**, 669 (1966).

[10] Y. Ueda, Phys. Rev. **145**, 1214 (1966).

[11] P. Signell and D. Marker, in Proceedings of Williamsburg Conference on Intermediate Energy Physics, 1966, Vol. II, p. 667 (unpublished).

[12] A. Simon, Phys. Rev. **79**, 573 (1950).

[13] R. Wilson, Phys. Rev. **85**, 563 (1952).

[14] D. Cohen, B. J. Moyer, H. C. Shaw, and C. N. Waddell, Phys. Rev. **130**, 1505 (1963).

[15] J. A. Edgington and B. Rose, Nucl. Phys. **89**, 523 (1966).

[16] W. C. Beckham, University of California Radiation Laboratory Report No. UCRL-7001, 1962 (unpublished).

[17] A. F. Kuckes, R. Wilson, and P. F. Cooper, Jr., Ann. Phys. (N. Y.) **15**, 193 (1961).

[18] J. A. Edginton and B. Rose, Phys. Letters **20**, 552 (1966).

[19] G. F. Chew, Phys. Rev. **80**, 196 (1950).

[20] R. J. Glauber, Phys. Rev. **100**, 242 (1955).

interactions between the final-state nucleons and the spectator particle, we would expect only two types of final states:

$$p+d \rightarrow n_s+p+p+\gamma \quad (\text{quasifree } pp\gamma), \quad (2.1)$$

$$p+d \rightarrow p_s+n+p+\gamma \quad (\text{quasifree } pn\gamma). \quad (2.2)$$

(The subscript s refers to the spectator nucleon.) A special case of (2.2) is the reaction

$$p+d \rightarrow p_s+d+\gamma$$
$$(\text{quasifree } pn \text{ radiative capture}), \quad (2.3)$$

in which the n-p system ends up in the bound $^3S_1$ final state. This process will be treated apart from n-p bremsstrahlung in the experiment. It is of interest in itself since it represents a way of studying the time-reversed reaction to deuteron photodisintegration.

If we now "turn on" final-state interactions, two more final states will be formed:

$$p+d \rightarrow p+d+\gamma \quad (pd\gamma), \quad (2.4)$$

$$p+d \rightarrow \text{He}^3+\gamma \quad (\text{He}^3\gamma). \quad (2.5)$$

Final state (2.4) will be produced at the expense of both (2.1) and (2.2), while the formation of final state (2.5) will reduce all other cross sections. Finally, we must allow for the possibility of rescattering of the final-state nucleons:

$$p+d \rightarrow p+n+p+\gamma \quad (\text{multiple-scattering term}). \quad (2.6)$$

The cross sections for the production of final states (2.1)–(2.4) can be expressed in terms of the fundamental interactions as follows:

$$\sigma_{\text{qf } pp\gamma} = K_1 \sigma_{pp\gamma},$$
$$\sigma_{\text{qf } pn\gamma} = K_2 \sigma_{np\gamma},$$
$$\sigma_{\text{qf cap}} = K_3 \sigma_{\text{cap}},$$
$$\sigma_{pd\gamma} = \tfrac{3}{4} |F(q^2)|^2 (\sigma_{pp\gamma}+\sigma_{np\gamma}).$$

The constants K_i allow for the cross-section reduction due to Glauber shielding and final-state interactions; the spin factor of $\tfrac{3}{4}$ times the square of the deuteron form factor $|F(q^2)|^2$ represents the likelihood that a bound deuteron is formed in final state (2.4). The cross section for the formation of final state (2.5) is known to be small, and we shall use the results of a recent measurement performed[21] at 156 MeV as an upper limit at our energy. Channel (2.6) cannot be readily related to fundamental $NN\gamma$ processes.

In this experiment we identified events from final states $p+d \rightarrow p+d+\gamma$ (a 3-constraint fit), $p+d \rightarrow n_s+p+p+\gamma$, and $p+d \rightarrow p_s+d+\gamma$ (both 0-constraint fits). Final state $p+d \rightarrow p_s+n+p+\gamma$ could not be identified, but we obtained its contribution by sub-

tracting the identified channels from the measured total rate. The validity of applying the impulse approximation to radiative interactions was tested by comparing the results from reactions (2.1) and (2.3) with the corresponding free channels which are known. The values for K_1 and K_3 found in this way were subsequently used to determine K_2, which allowed the conversion of $\sigma_{\text{qf } pn\gamma}$ to $\sigma_{np\gamma}$. An alternative, though less reliable, way to determine $\sigma_{np\gamma}$ follows from the expression for $\sigma_{pd\gamma}$ and was employed as well.

III. EXPERIMENTAL METHOD

The purpose of this experiment was to identify the various final states as unambiguously as possible. The emission of a γ ray sets all of them apart from the large background of elastic and quasielastic scattering eveuts. Hence its detection was made the central point of our approach. For the detection of the charged particles in coincidence with the γ ray we used spark chambers, since they could provide us with good direction and reasonable range information over large solid angles. Our apparatus did not detect neutrons, He^3, and spectator protons, and it did not identify the detected charged particles as protons or deuterons. The major components of the experimental setup are described in the following paragraphs.

Beam

This experiment was performed in the external proton beam of the University of Rochester 130-in. cyclotron. The beam is extracted by scattering from an internal carbon target, thus achieving a vertical polarization of 92%. After being brought to the experimental area by a quadrupole and bending-magnet combination, the beam was trimmed to size by brass slits. We made use of the improved duty cycle (30%) of the cyclotron provided by the recently installed stochastic acceleration system.[22] The final beam had an intensity of 2×10^7 protons/sec. Its energy at the center of the target was 197 ± 5 MeV, as determined by range in copper, using the range-energy relations of Rich and Madey.[23]

The beam intensity was monitored with a thin-foil ion chamber placed downstream of the target. It was calibrated several times during the experiment by observing p-p elastic-scattering events in a separate telescope and using the recent p-p cross-section and polarization data of Marshall.[24] Corrections for nuclear absorption in the elements of the calibration telescope were applied. The separate calibrations were consistent to within 7%. No short-term drifts exceeding this uncertainty were detected.

[21] D. Bachelier, M. Bernas, I. Brissaud, C. Detraz, J. P. Didelez, H. Langevin-Joliot, J. Lee, and P. Radvanyi, Phys. Letters 21, 697 (1966).

[22] E. Nordberg, IEEE Trans. Nucl. Sci. NS-12, 973 (1965).
[23] M. Rich and R. Madey, University of California Radiation Laboratory Report No. UCRL-2301, 1954 (unpublished).
[24] J. F. Marshall, C. N. Brown, and F. Lobkowicz, Phys. Rev. 150, 1119 (1966).

Target

The deuterium target was of standard design. The liquefied gas was contained in a target cup in the shape of a vertical right circular cylinder of 2 in. diam, with a wall made of 0.003-in.-thick Mylar foil. The vacuum wall surrounding the cup was made of 0.064-in.-thick Al, and entrance and exit windows were cut out of the metal and covered with 0.005-in.-thick Mylar in order to keep the material in the path of the direct beam to a minimum. These precautions were taken to keep down radiative background rates from two possible sources: π^0 production and nuclear bremsstrahlung by the beam protons in heavy nuclei.

Several times during the course of the experiment the deuterium in the target cup was replaced by liquid hydrogen in order to determine background rates from a target free of neutrons.

Gamma Counter

A diagram of the 4-element telescope which constituted the γ counter is shown in Fig. 1. The detected particle must enter through the veto counter ($\bar{1}$) as neutral and must convert to one or more charged particles in the Cu converter. The conversion product(s) must be charged in order to register in the scintillation counters (2) and (4), and must have a velocity $\beta \geqslant 0.75$ in order to be seen in the water Čerenkov counter (3). A γ ray converting in the Cu into an e^+-e^- pair would show up with the correct signature $\bar{1}234$ if at least one of the electrons reached counter (4).

The detection efficiency as a function of γ energy was calculated by a Monte Carlo program and measured with a tagged photon beam at the Cornell 1.9-BeV electron synchrotron. Figure 2 shows the results of both procedures. The measured points can only serve as a check on the shape of the curve since their over-all normalization was subject to a systematic uncertainty of ±25%.

This γ counter did not provide any information about the energy of a detected γ ray, except that E_γ exceeded
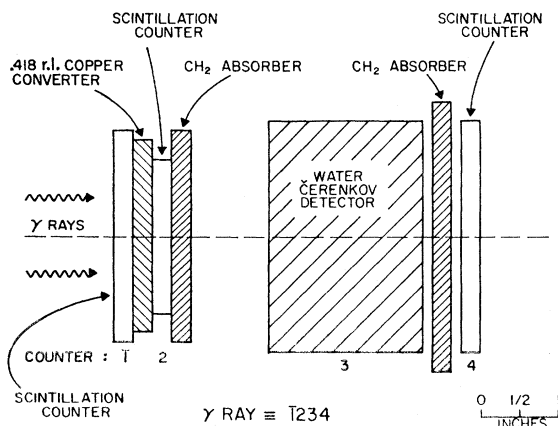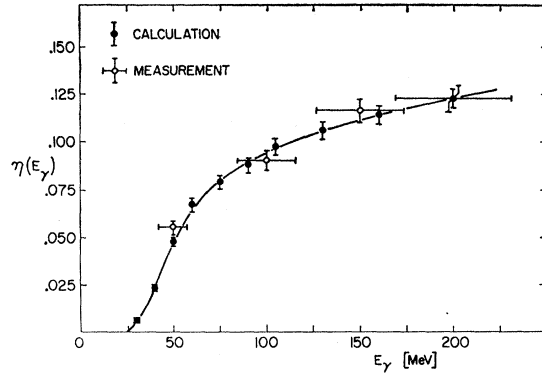
FIG. 2. The detection efficiency of the γ counter as a function of γ energy. In addition to the statistical errors shown, the measured points are subject to a systematic uncertainty of ±25%.

the threshold of about 40 MeV. Its direction definition was ±9.5°, both vertically and horizontally. The solid angle subtended by the γ counter could not be found in the standard manner because of the uncertainty as to which of its elements acted as the defining counter. The efficiency program was thus written to calculate the product $\Delta\Omega_\gamma \times \eta_\gamma$ as a function of E_γ; the finite extent of the target volume traversed by the beam was folded in.

An easy test for the fact that the γ counts were indeed caused by γ rays was to remove the converter; this always reduced the counting rate by about 85%. The sensitivity of the γ counter to neutrons was tested by placing it at 45° to the beam with the D_2 target full. Al, Cu, and Pb absorbers of different radiation lengths were placed between the target and the veto counter. The counting rate was found to decrease exponentially with increasing radiation length in the manner expected only for γ rays lost through conversion in the absorber. The Čerenkov counter provided a strong rejection criterion for heavy charged particles which managed to sneak through the veto counter. The proton-rejection ratio of the Čerenkov counter was measured to be 10^{-5}.

Detection of Charged Particles

While the first three items discussed in this section were applicable to the detection of all the final states resulting from quasifree N-N bremsstrahlung, we shall now describe the different arrangements which were designed and used for the detection of the individual final states. The members of final state (2.4) exhibit three-body kinematics which can be overdetermined by detecting both charged particles, thus permitting us to determine *ex post facto* which was the proton and which the deuteron. Although final state (2.1) consists of four particles, the spectator neutron does not take part in the collision according to our model, so that the two protons and the γ ray exhibit three-body kinematics which are smeared some by the initial momentum of the target proton. The kinematics of all four particles can be just determined by detecting both protons along

SCINTILLATION COUNTER

.418 r.l. COPPER CONVERTER   CH₂ ABSORBER   CH₂ ABSORBER

WATER ČERENKOV DETECTOR

γ RAYS

COUNTER : $\bar{1}$ 2   3   4

SCINTILLATION COUNTER

γ RAY $\equiv \bar{1}234$

0   1/2   1
INCHES

FIG. 1. The γ-counter telescope.
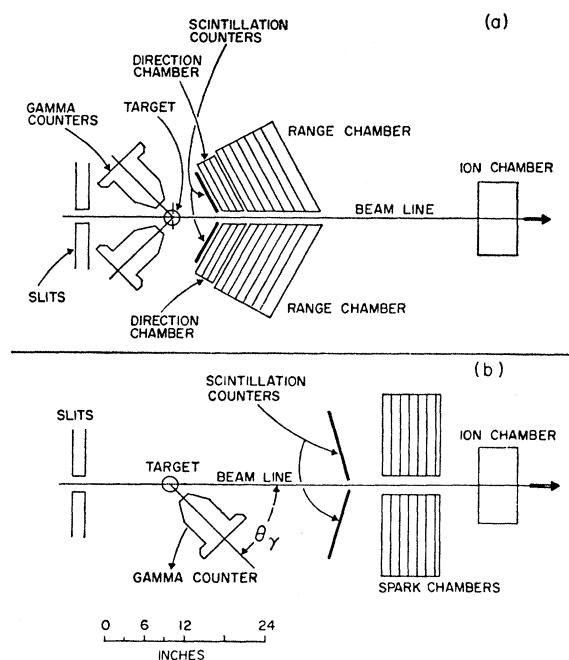
FIG. 3. Top views of the apparatus. (a) The spark chambers used for the detection of two-track events. (b) The spark chambers used for the detection of one-track events.

with the γ ray. Because the energy of the spectator protons in final state (2.2) is below a possible detection threshold, and since the neutron could not be detected with sufficient efficiency to produce acceptable counting rates, we were unable to kinematically determine this final state. Final state (2.3) is expected to exhibit two-body kinematics which are smeared by the initial motion of the target neutron. Thus, for a fixed γ direction, the deuteron will be pitched into a narrow forward cone on the opposite side of the beam from the γ ray. The detection of the deuteron permits the kinematic determination of these events.

On the basis of these considerations, we employed two sets of spark chambers during separate runs of this experiment. The arrangement shown in Fig. 3(a) was used in Run V for the detection of two-track events from final states (2.1) and (2.4). Except for minor modifications, the spark chambers used were the same combination of direction and range chambers which had been employed in our $pp\gamma$ experiment.[4] The average energy resolution of the range chambers was 12%. Two identical γ counters were used in order to double the event rate. The spark chambers were triggered only by a fast coincidence between either γ counter and the large-area scintillation counters 5 and 6. Code lights appearing on the film record of each event indicated which of the two γ counters had been involved in the trigger. The two γ counters were frequently interchanged during the run in order to average out any possible difference in their performance. The mirrors permitted a 90° stereo view of both sets of chambers to

be recorded by a single overhead camera. The γ counters were placed alternately at laboratory angles of 90° and 135°.

The arrangement shown in Fig. 3(b) was used in Run IV for the detection of the deuterons in final state (2.3). Each of the two identical plate assemblies consisted of 21 Al plates whose thickness varied from 0.025 (front plate) to 0.125 in. (back plate). The average energy resolution was 4.5%. The direction of the particle was obtained by connecting the first few sparks of its track to the center of the target. The error incurred by assuming that the particle came from the target center was smaller than the rms error due to multiple Coulomb scattering. Both plate assemblies were fired by a fast coincidence between the γ counter and a charged particle in either one of the scintillation counters 5 or 6 which covered the sensitive solid angle of the spark-chamber plates. Code lights appearing on the film record of each event indicated the type of trigger which had occurred. The mirrors permitted a 90° stereo view of each plate assembly to be recorded by a single overhead camera. The γ counter was alternately placed at laboratory angles of 45°, 90°, and 135°, both north and south of the beam.

Prior to these two spark-chamber runs, we performed a preliminary study of coincidence rates between the γ counter and one or two charged particles as detected by scintillation counters 5 and 6, which were located as shown in Fig. 3(a). These counter data were also used later in the analysis.

Electronics

Schematic diagrams of the electronic logic used in the two spark-chamber runs are shown in Figs. 4(a) and 4(b). All of the fast logic circuitry consisted of standard chronetics modules. The outputs marked FCC set the code lights and triggered the film-advance system. A fast "gate trigger" deactivated all coincidence circuits during the spark-chamber discharge in order to prevent rf pickup from invalidating the scaler data. The delay of 52 nsec (equal to one period of revolution of the beam at the target radius) was introduced to monitor random rates continuously.

Data Collection

In order to be able to monitor the time stability of the detection system, the data were accumulated during many short data runs which typically lasted 1 h. The angular position of the γ counters was changed frequently between such runs. Periodically, we emptied the liquid D_2 from the target cup in order to measure background rates, both with an empty target and with the cup filled with liquid H_2. About 10% of the total data-collection time was spent on background measurements.
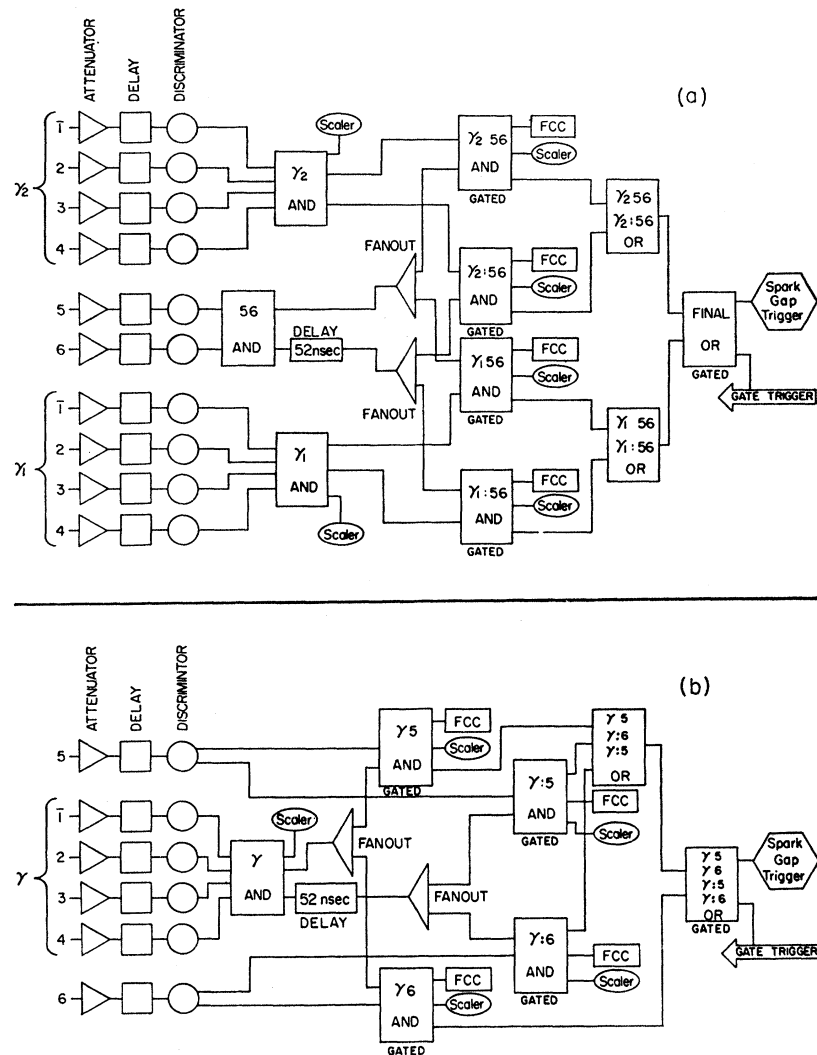
FIG. 4. Schematics of the electronic logic. (a) The spark chambers of Fig. 3(a) are triggered by the coincidence between a γ ray and two charged particles. (b) The spark chambers of Fig. 3(b) are triggered by the coincidence between a γ ray and a single charged particle.

IV. DATA REDUCTION

Counter Data

All measured coincidence rates were corrected for the contributions from random coincidences as monitored and normalized to a given total beam flux. Subtraction gave "D_2-H_2" and "D_2-empty" rates. Averaged over all coincidence rates, the random corrections amounted to about 15%, while the background subtractions were typically 30% of the total rates.

The rates observed for a fixed θ_γ were grouped into the following categories: (γ) is the total γ counts; $(\gamma A)_C$ is the coincidences between a γ ray and a single charged particle on the opposite side of the beam; $(\gamma T)_C$ is the coincidences between a γ ray and a single charged particle on the same side of the beam; and $(\gamma A T)_C$ is the coincidences between a γ ray and one charged particle on each side of the beam. The subscript C refers to the

location of the counters 5 and 6 close to the target, as shown in Fig. 3(a). It is replaced by F when referring to the counter configuration of Fig. 3(b).

Two-Track Events

The film exposed during Run V was scanned for frames which showed a pair of tracks. 58% of the total did. These were digitized and reconstructed. The pair of tracks was required to originate from a vertex within the volume of the D_2 target. The surviving sample was first fitted kinematically to the $pd\gamma$ hypothesis. Our measurement of eight kinematic quantities overdetermined this three-particle final state three times, once we had picked a mass assignment. Keeping only the direction of the γ ray fixed, a computer program performed a 3-constraint fit on the directions and energies of the two charged particles. The parameter used as a measure
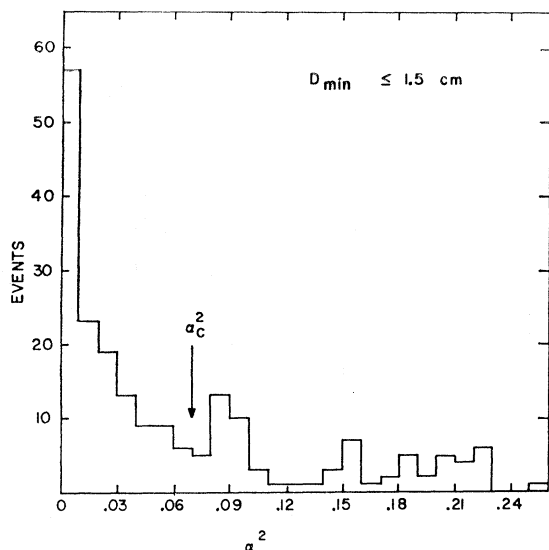
FIG. 5. Distribution of the minimum fitting parameter α^2 for two-track events. D_{min} represents the distance of closest approach of the two tracks in the target, and the above condition ensures their origin from a common vertex.

of the "goodness of fit" was

$$\alpha^2 = \sum_{i=1}^{2} \{2(1-\cos\beta_i)+F[(T_i{}^M - T_i{}^C)/T_i{}^C]^2\},$$

where β_i is the space angle between the measured and the calculated direction of particle i, and $T_i{}^M$ and $T_i{}^C$ are its measured (from range) and calculated energies, respectively. The weight factor F was chosen so that the experimental uncertainties in the direction and range determinations contributed about equally to α^2. We used $F=0.5$ throughout. Each of the two possible mass assignments was processed in this manner, and the one which resulted in the smaller value for α^2 was chosen as the correct one.
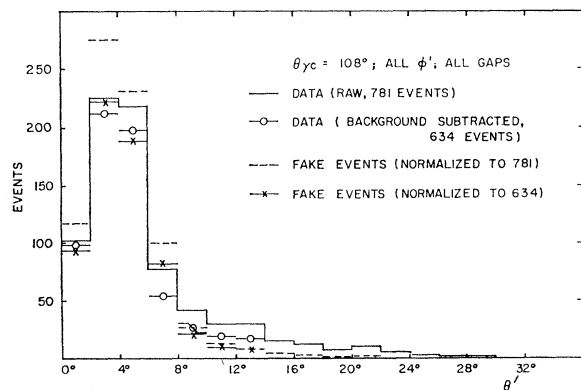
FIG. 6. Comparison of the θ' distribution exhibited by the one-track events with a prediction from a quasifree-pn radiative-capture model. The data are shown before and after the application of the background correction.

The distribution of the smaller values for α^2 for all events is shown in Fig. 5. On the basis of the experimental uncertainties in the determination of the directions and ranges of the two charged particles, a value of $\alpha^2 \cong 0.03$ was expected. Since the distribution is still falling off beyond that point, we chose $\alpha^2 = 0.07$ as our cutoff, i.e., all events with $\alpha^2 \leqslant 0.07$ were accepted as $pd\gamma$ events. There was a total of 284 such events.

The two-track events corresponding to quasifree $pp\gamma$ were extracted on the basis that they had to be poor fits to the $pd\gamma$ hypothesis, and we required $\alpha^2 \geqslant 0.10$. A total of 136 such events was found.

The events having $0.07 < \alpha^2 < 0.10$ could not be assigned to $pd\gamma$ or qf $pp\gamma$ on an individual basis. Instead, we corrected the cross sections calculated for these processes for events lost by the above procedure. (See Sec. V.)

One-Track Events

The film exposed during Run IV was scanned for frames showing a single track coming from the target and appearing on the side of the beam indicated by the codelight. 47% of the total did. The geometrical arrangement of the spark chambers and mirrors enabled us to measure these pictures by hand on the scanning table to good accuracy.

Owing to the presence of the spectator proton, these measurements provided only a 0-constraint fit to the kinematics of final state (2.3), thus preventing the selection of good events on an individual basis. We employed the following procedure for estimating the background contribution in our sample. For every fixed γ direction the measured tracks were reconstructed in a spherical coordinate system (θ',ϕ') whose polar axis pointed in the direction which the deuteron would take if the target neutron were at rest $(p_S=0)$. The azimuthal angle was defined so that the γ ray emerged with $\phi'=\pi$. Summing over all ϕ', we obtained a distribution of the data in θ' which was compared to a distribution of "fake" events generated on a computer by a Monte Carlo program according to our theoretical model; the momentum distribution of the target nucleon was derived from the Hulthén wave function,[17] and the emerging deuterons had to strike the sensitive region of the spark chambers; the directional smearing caused by multiple Coulomb scattering and the range uncertainty caused by the finite resolution of the spark-chamber gaps and by the finite size of the target were also folded in. When the two distributions were fitted in the angular region $\theta' \leqslant 8°$, the data contained an excess of events for $\theta' > 8°$, which was taken as a measure of the background contained in our data sample. The background subtraction in the region $\theta' \leqslant 8°$ amounted to 7.5%, reducing our total sample of quasifree-pn radiative-capture events to 696. This procedure is illustrated in Fig. 6. (The restriction of the data sample to this limited region in θ' is justified by the fact that it contained $\sim 90\%$ of all

expected good events, but only ∼30% of the total background seen in the spark chambers.) The validity of our model is further supported by a close agreement between the ϕ' distributions (summed over $\theta' \leqslant 8°$) of the data and of the generated "fake" events.

V. RESULTS

Quasifree $pp\gamma$

The final state of the reaction $p+d \rightarrow n_s+p+p+\gamma$ is described by eight independent kinematic variables. We chose the momentum of the spectator ($\mathbf{p}_s$), the direction and energy of the γ ray ($\theta_{\gamma c}, \phi_{\gamma c}, E_{\gamma c}$), and the direction ($\theta_c, \phi_c$) of the momentum vector $\Delta\mathbf{p}_c = \mathbf{p}_{1c} - \mathbf{p}_{2c}$. The labels γ, 1, and 2 identify the particles, while the subscript c refers the last five quantities to the center-of-mass (c.m.) coordinate system of the two protons before the interaction. This choice facilitates comparisons of the quasifree-$pp\gamma$ data with our previous free-$pp\gamma$ results. Because the transformation between the system C and the laboratory depends on $\mathbf{p}_s$, and because of difficulties due to resolution and detection efficiency, the comparisons could not be made directly. Instead, we generated (for a fixed γ direction) "fake" quasifree-$pp\gamma$ events with a Monte Carlo program according to the $E_{\gamma c}$, $\cos\theta_c$, and ϕ_c distributions found in the free-$pp\gamma$ analysis, and folded in the smearing caused by the spectator momentum (calculated from the Hulthén wave function) and the experimental uncertainties. In order to be classified as a "hit," both final-state protons of the "fake" event had to have the proper directions and sufficient energy to be detected in the spark chambers as a two-track event. The "hits" were subsequently analyzed in the same manner as the actual events, and the resulting c.m. distributions were compared with the observed histograms, after proper normalization. This procedure is illustrated in Figs. 7(a)–7(c) for the distributions in $E_{\gamma c}$, $\cos\theta_c$, and ϕ_c. The ranges of the variables $\cos\theta_c$ and ϕ_c have been reduced by folding about $\cos\theta_c = 0$ and $\phi_c = \frac{1}{2}\pi$, as allowed by the identity of the protons. We were able to further improve the statistical meaning of these comparisons by combining the data taken at $\theta_{\gamma c} = 108°$ and 147°. This was possible only because the c.m. distributions found in the $pp\gamma$ experiment for those two angles were indistinguishable.

The excess of measured events having $E_{\gamma c} < 20$ MeV [in addition to a total of 12 events having $E_{\gamma c} < 0$ MeV which are not shown in Fig. 7(a)] points to some contamination in the sample, which could be caused by random coincidences between a γ-ray and a quasielastic pp scattering event. Such an origin suggests a decreasing background contribution with increasing γ energy. Apart from the low end of the $E_{\gamma c}$ distribution, we find reasonably good agreement between the quasifree-$pp\gamma$ data and the predictions based on the $pp\gamma$ results.

This is also true for the $\cos\theta_c$ and the ϕ_c distributions, where only events having $E_{\gamma c} \geqslant 20$ MeV are shown. In
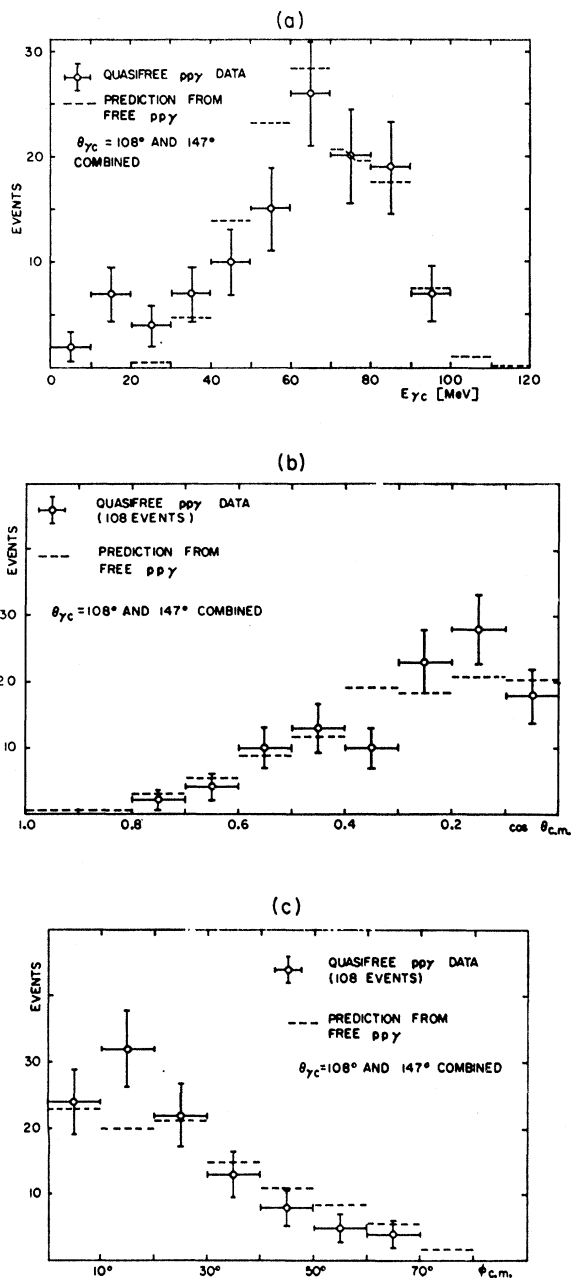
FIG. 7. Comparison of the c.m. distributions between the quasifree-$pp\gamma$ data and predictions from free $pp\gamma$ in the variables (a) $E_{\gamma c}$, (b) $\cos\theta_c$, and (c) ϕ_c.

both experiments, performed with nearly identical apparatus, some features of these angular distributions were due to the energy and range limitations imposed by the spark chambers: For $\cos\theta_c > 0.6$ one of the protons fails to meet the minimum range requirement, and events are lost into the gap between the spark chambers for $\phi_c > 50°$ (if the γ counter is placed in the horizontal plane). However, there is evidence from both experiments which suggests that the distributions in

TABLE I. Differential cross sections for quasifree and free $pp\gamma$, integrated over $E_\gamma^{lab} \geqslant 40$ MeV, and expressed in the $pp\gamma$ c.m. system.

		$\theta_{\gamma c}=108°$	$\theta_{\gamma c}=147°$
$(d\sigma/d\Omega_\gamma)_{qf\ pp\gamma}{}^{c.m.}$	[nb sr^{-1}]	22.4 ± 4.7	33.2 ± 9.7
$(d\sigma/d\Omega_\gamma)_{free\ pp\gamma}{}^{c.m.}$	[nb sr^{-1}]	47.4 ± 2.7	63.8 ± 7.4

Average (quasifree/free) ratio: $K_1 = 0.50\pm0.10$.

neither c.m. angle are purely isotropic: They show a preference for large θ_c and small ϕ_c.

Further evidence for the fact that we were indeed dealing with an almost pure sample of quasifree-$pp\gamma$ events was obtained from the momentum spectrum of the spectator neutrons. The distribution calculated from the data is shown in Fig. 8, together with predictions based on the Hulthén wave function, before and after the experimental resolutions have been folded in. While the agreement for $p_s \leqslant 1.0$ F^{-1} is good, there exists a small excess of events with large spectator momentum. This could be caused by the background mentioned earlier. The smallness of the excess of events having large spectator momentum is also an indication that the rescattering channel (2.6) is small.

The differential cross sections for quasifree $pp\gamma$ were calculated at $\theta_{\gamma c}=108°$ and $147°$ by using the information provided by the "fake" generator program to make the proper corrections for events lost as a result of the direction and range limitations imposed by the spark chambers and as a result of the selection criterion $\alpha^2 \geqslant 0.10$. The program also provided us with the value for the γ-counter efficiency averaged over the "hits." The resulting c.m. cross sections are quoted in Table I, together with the free-$pp\gamma$ results obtained earlier. These numbers imply an average value of $K_1 = 0.50\pm0.10$.

Quasifree pn Radiative Capture

Before we can interpret the number of events contained in the forward cone with $\theta' \leqslant 8°$ in terms of differential cross sections and asymmetries for the
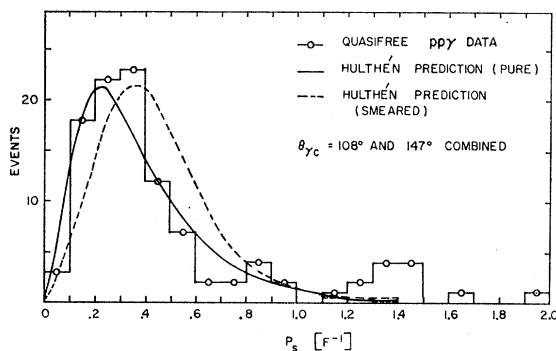
FIG. 8. The spectator-momentum spectrum derived from the quasifree-$pp\gamma$ events. The solid curve shows a pure prediction from the Hulthén wave function; folding in the experimental resolutions results in the dashed curve.
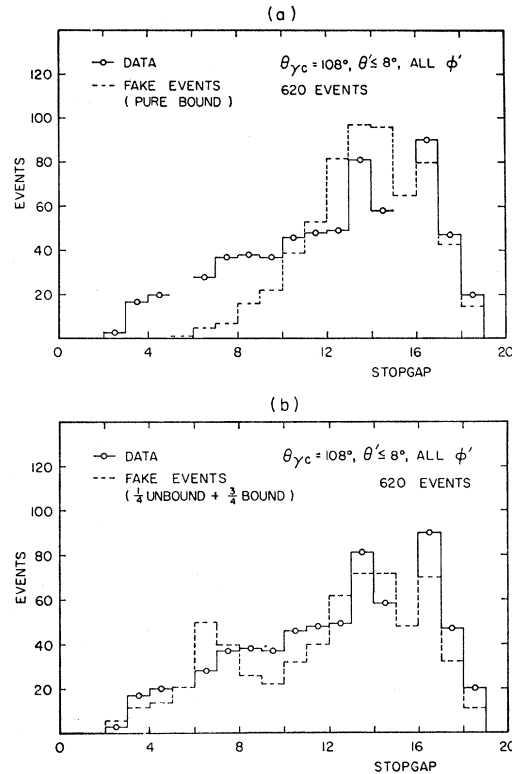
FIG. 9. Range distribution of the charged particles observed in the events from quasifree pn radiative capture. (a) Comparison with "fake" events consisting of bound final states only. (b) Comparison with "fake" events consisting of a 1:3 mixture of unbound and bound final states. (The missing data entries in bins 6 and 16 are not due to a real effect in the spark chambers. They were caused by an accidental rounding procedure during the data handling which produced a slight shift in the range values.)

reaction $p+d \rightarrow p_s+d+\gamma$, we must give evidence that the observed charged particles were deuterons. While the spark-chamber data did not give this information directly, they provided some indirect evidence in the form of the range distribution inferred from the last gap traversed by the particle ("stopgap"). Comparing the distribution observed for a fixed γ direction with the one obtained for the fake events which were generated on a computer under the assumption that a bound deuteron was formed, we found a noticeable excess of events with too little range, as shown in Fig. 9(a). The number of excess events is far greater than can be explained by the probability that the deuteron underwent nuclear absorption before reaching the end of its natural range. We believe that this effect is caused by quasifree-pn radiative-capture processes in which the final state of the pn system is not the bound $^3S_1$ state of the deuteron, but instead an unbound $^1S_0$ or $^3S_1$ state, in which the relative energy of the two nucleons is very small. Such final states would exhibit the same kinematic characteristics as the bound final states, but they would interact with the detection apparatus as a proton of half the energy which the deuteron would have, and

TABLE II. Differential cross sections for quasifree-pn radiative capture, and predictions for inverse deuteron photodisintegration, expressed in the $d\gamma$ c.m. system. The uncertainties quoted for the predictions represent the range of values calculated in Ref. 26 for various forms of the deuteron wave function.

	$\theta_{\gamma c}=60°$ [μb sr^{-1}]	$\theta_{\gamma c}=108°$ [μb sr^{-1}]	$\theta_{\gamma c}=147°$ [μb sr^{-1}]
$(d\sigma/d\Omega)_{\text{qfcap.}}^{\text{c.m.}}$ (bound state)	0.80±0.15	0.55±0.10	0.32±0.07
$(d\sigma/d\Omega)_{\text{qfcap.}}^{\text{c.m.}}$ (unbound state)	0.18±0.05	0.12±0.03	0.07±0.02
$(d\sigma/d\Omega)_{p+n\rightarrow d+\gamma}^{\text{c.m.}}$ (prediction)	1.00±0.10	0.78±0.12	0.46±0.07

Average (quasifree/free) ratio: $K_3=0.75\pm0.15$.

hence they would stop earlier in the spark chamber. (The average transverse momentum of the unbound nucleons must be small enough to preserve the observed peaking in the θ' distribution; this implies that the two nucleons have a relative energy $E_R\leqslant 1.5$ MeV.) We generated fake events representing these unbound final states on the assumption that the pn system had zero relative energy. By fitting our range data to distributions representing mixtures of fake events in the bound and the unbound state [Fig. 9(b)], we were able to separate the two groups. The average branching ratio of unbound to bound final states was found to be $\alpha=0.22\pm0.04$.

Positive identification of the deuterons from quasifree pn radiative capture was established in a separate run as follows: With the γ counter at $\theta_{\gamma c}=77°$, we aligned a four-counter telescope along $\theta'=0°$. The charged particle detected in coincidence with a γ ray was analyzed for its time of flight and total energy by an on-line PDP8 computer.[25] The 36 events which were obtained are displayed in Fig. 10. The dashed line separates the proton and deuteron regions, as established by calibration runs with elastically scattered deuterons. The detected particles are cleanly divided into 32 deuterons and 4 protons. Unfortunately, the proton-detection threshold of the telescope was higher than that of the spark chambers, so that fewer of the unbound state events could be detected. The two protons in the lowest-energy channel show the same flight time as the deuterons and are thus strong candidates for the unbound state.

The differential cross sections for quasifree pn radiative capture in the bound and the unbound final state were calculated in the p-n c.m. system. They are summarized in Table II, together with predictions for the formation of the bound final state derived from the reaction[26] $\gamma+d\rightarrow p+n$ by detailed balance. Our results imply an average value of $K_3=0.75\pm0.15$.

Apart from the presence of the spectator proton, the reaction $p+d\rightarrow p_s+d+\gamma$ is the time-reversed channel of the reaction $\gamma+d\rightarrow p+n$. Hence the γ-ray asymmetry resulting from a polarized proton beam in our case should be equal to the final polarization of the protons resulting from photodisintegration with an un-

polarized γ beam. While the latter quantity has been predicted theoretically,[26] it has so far not been measured. The present experiment used a polarized proton beam and offered a convenient way to test these predictions. It was an easy matter to determine the right-left asymmetry of the quasifree-pn radiative-capture reaction, both for the bound and the unbound final state, from our data. The results are listed in Table III; they have been normalized to a beam polarization of 1.00. Predictions for the proton polarization are also shown. Our data are in good agreement, although they prefer to lie below the predictions. The asymmetries for the unbound state are afflicted with large uncertainties, caused chiefly by the small number of events in the sample. They tend to exhibit smaller asymmetry values than the bound-state events.

$pd\gamma$

In order to describe the kinematics of the final state of the reaction $p+d\rightarrow p+d+\gamma$, we chose the following five independent variables: the direction and energy of the γ ray $(\theta_{\gamma c},\phi_{\gamma c},E_{\gamma c})$ and the direction (θ_c,ϕ_c) of the momentum vector $\Delta\mathbf{p}_c=\mathbf{p}_{pc}-\mathbf{p}_{dc}$. The subscripts γ, p, and d identify the particles, while the letter c indicates that all quantities are expressed in the p-d c.m. system before the collision. The direction of the incident beam forms the polar axis, and ϕ_c is measured relative to the plane defined by the momenta of the incident proton
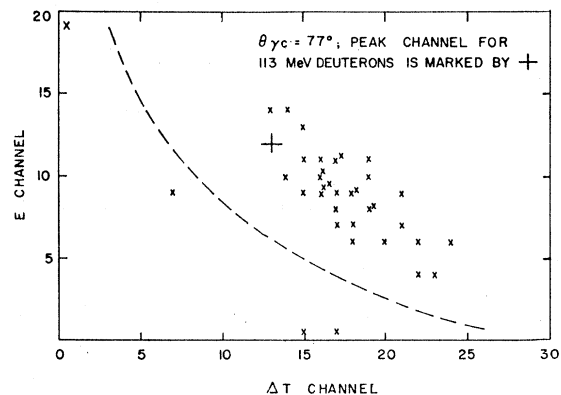
FIG. 10. Scatter plot of the total-energy and time-of-flight coordinates of the charged particles observed in coincidence with the γ ray by a telescope placed at $\theta'=0°$.

[25] The details of this system are described by R. E. Adelberger, Ph.D. thesis, University of Rochester, 1967 (unpublished).

[26] A. Donnachie and P. J. O'Donnell, Nucl. Phys. 53, 128 (1964).
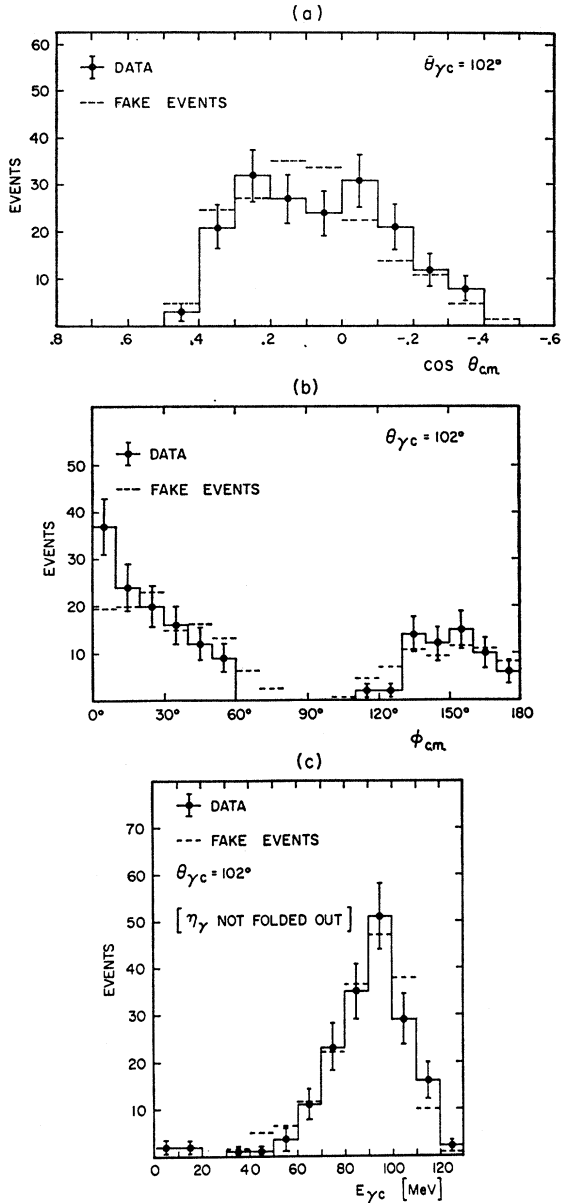
FIG. 11. Comparison of the c.m. distribution from the $pd\gamma$ events at $\theta_{\gamma c}=102°$ with predictions from our preferred set of functional forms in the variables (a) $\cos\theta_c$, (b) ϕ_c, and (c) $E_{\gamma c}$. [The γ-counter efficiency $\eta(E_\gamma)$ has *not* been folded out of the $E_{\gamma c}$ distributions shown.]

and the γ ray. The variables θ_c and ϕ_c vary over the ranges $-1\leqslant\cos\theta_c\leqslant1$ and $0\leqslant\phi_c\leqslant\pi$, and no further folding is possible.

The limitations on the directions and ranges of the proton and deuteron imposed by our detection system severely reduced the detectable phase space. The deuteron threshold excluded the region $\cos\theta_c>0.6$, and the proton threshold excluded the region $\cos\theta_c<-0.5$; events with ϕ_c near $\frac{1}{2}\pi$ (for the γ counter in the horizontal plane) are likely to be lost into the gap between the chambers. Furthermore, the probability that the

TABLE III. γ-ray asymmetries for quasifree-pn radiative capture, and predictions for inverse deuteron photodisintegration. The measured asymmetries have been normalized to a beam polarization of 1.00. The uncertainties quoted for the predictions represent the range of values calculated in Ref. 26 for various forms of the deuteron wave function.

$\theta_{\gamma c}$	ϵ_γ (bound)	ϵ_γ (unbound)	ϵ_γ (predicted)
60°	-0.11 ± 0.08	$\cdots$	0.00 ± 0.02
77°	-0.28 ± 0.20[a]	$\cdots$	-0.09 ± 0.01
108°	-0.30 ± 0.06	-0.25 ± 0.18	-0.28 ± 0.02
147°	-0.41 ± 0.14	$+0.10\pm0.24$	-0.36 ± 0.03

[a] Measured with separate deuteron telescope.

deuteron will recombine after the two-nucleon interaction is given by the square of the deuteron form factor, which decreases sharply with increasing momentum transfer q^2 to the deuteron.[27] Thus the more likely the deuteron was to have sufficient energy to be detected, the less likely it was to be formed.

In order to extract cross sections from the observed sample of $pd\gamma$ events it was necessary to determine the functional dependence on the variables $\cos\theta_c$, ϕ_c, and $E_{\gamma c}$, so that corrections for the contributions from the unobservable regions could be applied. Towards this end, we again turned to a Monte Carlo program which generated fake $pd\gamma$ events according to a variety of assumed distributions in the variables $\cos\theta_c$, ϕ_c, and $E_{\gamma c}$. Each fake event was weighted according to the square of the deuteron form factor, and the directions and ranges of the charged particles were smeared according to the observed experimental uncertainties. In order to qualify as a hit, an event had to have one charged particle strike each of the spark chambers with sufficient energy to be detected. These hits were subsequently analyzed in the same manner as the actual data, and by comparing their distributions in $\cos\theta_c$, ϕ_c, and $E_{\gamma c}$ with the observed histograms, we were able to select the following functional dependences as giving the best fit to the data at $\theta_{\gamma c}=102°$:

$$N(\cos\theta_c)=\tfrac{1}{2}(2-\cos\theta_c),\qquad[-1\leqslant\cos\theta_c\leqslant1]$$

$$N(\phi_c)=(1/2\pi)(3\pi-2\phi_c),\qquad[0\leqslant\phi_c\leqslant\pi]$$

$$N(E_{\gamma c})=\frac{1}{2}\left\{1+\frac{1}{12\sqrt{(2\pi)}}\exp\left[-\left(\frac{E_{\gamma c}-98}{12\sqrt{2}}\right)^2\right]\right\},$$

$$[40\leqslant E_{\gamma c}\leqslant127\text{ MeV}].$$

The comparisons between the data and the fake events generated according to these functional de-

TABLE IV. Differential cross sections for $pd\gamma$, integrated over $E_\gamma^{\text{lab}}\geqslant40$ MeV, and expressed in the $pd\gamma$ c.m. system.

	$\theta_{\gamma c}=102°$	$\theta_{\gamma c}=143°$
$(d\sigma/d\Omega_\gamma)_{pd\gamma}^{\text{c.m.}}$ (nb sr^{-1})	91 ± 12	78 ± 12

[27] J. I. Friedman, H. W. Kendall, and P. A. M. Gram, Phys. Rev. **120**, 992 (1960).

TABLE V. Summary of laboratory differential cross sections for the distinct final states resulting from quasifree N-N bremsstrahlung in deuterium. All entries represent integrals over $E_\gamma{}^{\text{lab}} \geqslant 40$ MeV, and the units are μb sr^{-1}.

Final state	$(d\sigma/d\Omega_\gamma)_{\theta_\gamma=45°}{}^{\text{lab}}$	$(d\sigma/d\Omega_\gamma)_{\theta_\gamma=90°}{}^{\text{lab}}$	$(d\sigma/d\Omega_\gamma)_{\theta_\gamma=135°}{}^{\text{lab}}$
$n_s+p+p+\gamma$	0.027 ± 0.006[a]	0.018 ± 0.004	0.018 ± 0.005
$p_s+d+\gamma$	$1.19\ \pm0.23$	$0.50\ \pm0.09$	$0.19\ \pm0.04$
$p_s+(np)$unbound$+\gamma$	$0.26\ \pm0.05$	$0.11\ \pm0.02$	0.043 ± 0.009
$p+d+\gamma$	0.138 ± 0.027[b]	0.087 ± 0.012	0.056 ± 0.009
$\text{He}^3+\gamma$ [c]	0.111 ± 0.024	0.159 ± 0.034	0.060 ± 0.013
$p_s+n+p+\gamma$	$4.10\ \pm0.82$	$1.79\ \pm0.36$	$0.83\ \pm0.17$

[a] This value was inferred from free $pp\gamma$.
[b] This value was derived by extrapolation from data at the two larger angles.
[c] These values were calculated from the results reported in Ref. 21.

pendences are shown in Figs. 11(a)–(c). The good agreement is violated in the bin $0 \leqslant \phi_c < 10°$, where the data lie almost three standard deviations above the prediction. Such a peaking is unlikely to be real, but we have been unable to find an instrumental reason for this behavior. One should keep in mind that these functional forms may be neither unique nor precisely determined by our data. The statistical accuracy of the data is poor (the sample of fake events generated was always at least four times larger than the data sample), and the detection efficiency of the apparatus restricted our observations to a small fraction of phase space. But the present data are sensitive enough to rule out isotropy in any of the variables $\cos\theta_c$, ϕ_c, and $E_{\gamma c}$. The quoted functional forms should be taken as an indication of the type of anisotropy exhibited by these data.

The small size of the data sample obtained at $\theta_{\gamma c}=143°$ (a total of 89 events) would render a similar analysis statistically meaningless. We found that the data at that angle were not inconsistent with the functional forms just determined at $\theta_{\gamma c}=102°$, and hence the same functional forms were used to correct the $\theta_{\gamma c}=143°$ data as well.

Using the fake generator program to provide us with the fraction of the total tries which were hits and with the average γ-counter efficiency for them, we calculated the c.m. differential cross sections for the $pd\gamma$ final state listed in Table IV. The program also found the average of the square of the deuteron form factor to be near 0.04 for the hits. The data were insufficient to permit the extraction of a meaningful asymmetry value.

Quasifree $np\gamma$

Up to this point, we have deduced differential cross sections, c.m. angular distributions, and γ-energy spectra for the following four final states:

$$n_s+p+p+\gamma, \tag{5.1}$$

$$p_s+d+\gamma, \tag{5.2a}$$

$$p_s+(np)\text{unbound}+\gamma, \tag{5.2b}$$

$$p+d+\gamma. \tag{5.3}$$

The final state

$$\text{He}^3+\gamma \tag{5.4}$$

was not identified in this experiment, since the He^3 did not have sufficient range to be detected. Instead we took the cross-section results obtained recently[21] at 156 MeV as an upper limit at our energy. For a comprehensive comparison between these different final states, we have listed their *laboratory* differential cross sections in Table V.

These results were fed into a Monte Carlo program which generated fake counter data for the coincidence rates (γ), $(\gamma A)_C$, $(\gamma R)_C$, $(\gamma A T)_C$, $(\gamma A)_F$, $(\gamma T)_F$, and $(\gamma A T)_F$ resulting from each of the final states. Since we had been able to distinguish between them experimentally, they were added incoherently, and their sum for each type of coincidence could be subtracted from the rate actually observed. According to Sec. II, we can attribute the excess in all categories except $(\gamma A T)_C$ and $(\gamma A T)_F$ to the final state $(p_s+n+p+\gamma)$. [Final state (2.6) is being neglected here, since it appears to be small.] The background subtraction was typically 40% of the single-charged-particle coincidences, leaving 60% to be interpreted as quasifree $pn\gamma$.

In order to deduce values for the quasifree-$pn\gamma$ cross sections from these excess counts, we generated fake counter data for the $(p_s+n+p+\gamma)$ final state for various assumed distributions in the variables $\cos\theta_c$, ϕ_c, and $E_{\gamma c}$ in the n-p c.m. system. The comparison between predicted and measured rates in the individual categories was then used to select the following preferred set of n-p c.m. distributions:

$$N(\cos\theta_c) = 1 - \cos\theta_c, \quad [-1 \leqslant \cos\theta_c \leqslant 1]$$

$$N(\phi_c) = 1, \quad [0 \leqslant \phi_c \leqslant \pi]$$

$$N(E_{\gamma c}) = \frac{1}{2}\left\{1 + \frac{1}{12\sqrt{(2\pi)}}\right.$$

$$\left. \times \exp\left[-\left(\frac{E_{\gamma c}-(E_{\gamma c}{}^{\text{max}}-12)}{12\sqrt{2}}\right)^2\right]\right\},$$

$$[40 \text{ MeV} \leqslant E_{\gamma c} \leqslant E_{\gamma c}{}^{\text{max}}].$$

($E_{\gamma c}{}^{\text{max}}$ is not constant because of the motion of the target neutron.) Note that the above functional forms should only be taken as an indication of the trends which our data exhibited. The form of $N(E_{\gamma c})$ was

TABLE VI. Inferred free-n-p-bremsstrahlung cross sections. The differential cross sections are quoted in the $np\gamma$ c.m. system. All cross sections represent integrals over $E_\gamma^{lab} \geqslant 40$ MeV. The errors listed in the last row do *not* include an estimate of the uncertainty due to theory.

Source of result	$\theta_{\gamma c}=60°$	$(d\sigma/d\Omega_\gamma)_{np\gamma}^{c.m.}$ [μb sr^{-1}] $\theta_{\gamma c}=108°$	$\theta_{\gamma c}=147°$	$\sigma_{np\gamma}^{total}$ [μb]
Quasifree $pn\gamma$, "high"	4.5±1.4	3.2±1.0	2.2±0.7	47±14
Quasifree $pn\gamma$, "low"	2.2±0.4	1.7±0.3	1.4±0.3	24±5
Quasifree $pn\gamma$, "best"	3.4±1.0	2.5±0.8	1.8±0.5	35±12
$pd\gamma$	⋯	2.7±0.4	3.2±0.5	⋯

suggested by the calculations of Cutkosky.[28] The laboratory differential cross sections for the $(p_s+n+p+\gamma)$ final state derived on the basis of these distributions are shown in the last row of Table V.

Since the separation between the final states $(p_s+n+p+\gamma)$ and $(p_s+(np)\text{unbound}+\gamma)$ is rather artificial, we have added them together to obtain cross sections for quasifree $pn\gamma$. In order to extract free-$np\gamma$ cross sections, we must infer a value for K_2 from our measurements of $K_1=0.50\pm0.15$ and $K_3=0.75\pm0.15$. In the case of quasifree $pp\gamma$, we imposed the stringent requirement of detecting two particles in coincidence with the γ ray, whereas only one must register in the case of quasifree $pn\gamma$. Hence we expect that a reduction factor of $\sqrt{K_1}=0.71\pm0.08$ would be more appropriate for quasifree $pn\gamma$. This argument is supported by the larger value of K_3. We have therefore taken $K_2=0.65\pm0.15$, where the large error was chosen to span the range of possible values. Using this correction factor, we arrived at the free-$np\gamma$ cross sections marked "high" in Table VI. However, these values must be considered to represent upper limits because of a bias in our treatment of background corrections. Whereas we have striven hard to obtain background-free samples of final states (5.1), (5.2), and (5.3), we have accepted *all* the excess in the counting rates for our quasifree-$pn\gamma$ sample. It could happen that an event belonging to final state (5.1), (5.2), or (5.3) will rescatter and hence be rejected. It could thus contribute a single-charged-particle coincidence count, while at the same time lowering the observed value of K_1 or K_3, and thus of K_2. Both effects would cause an increase in the deduced $np\gamma$ cross sections.

We obtained a lower limit for the $np\gamma$ cross sections by "turning off" all final-state interactions, i.e., by taking all $K_i=1$ and subtracting the full free contributions for final states (5.1) and (5.2) [final state (2.4) is excluded in this treatment] from the observed single-charged-particle coincidence rates. The excess was then interpreted as free $np\gamma$, leading to the cross sections marked "low" listed in Table VI.

We feel that these treatments indeed lead to upper and lower bounds, and hence we have taken their averages as our "best" values for the $np\gamma$ differential cross sections. They are listed in Table VI; their error bars are chosen to encompass both limits. Integration

over all γ directions on the basis of these three points leads to $\sigma_{np\gamma}^{total}=35\pm12$ μb for $E_\gamma^{lab}\geqslant40$ MeV.

By taking $\sigma_{pd\gamma}=(\sigma_{pp\gamma}+\sigma_{np\gamma})\frac{3}{4}|F(q^2)|^2$, we can use the $pd\gamma$ results to obtain $np\gamma$ cross sections by a different approach. Taking the $(\sigma_{np\gamma}/\sigma_{pp\gamma})$ ratio from the result just found, and using the average square of the deuteron form factor as given by our $pd\gamma$ analysis (~0.04), we arrive at the $np\gamma$ values listed in the last row of Table VI. The quoted errors do not include an estimate of the uncertainty in the theoretical method applied here, which is difficult to estimate but probably large. Consequently one should not derive too much comfort from the fair agreement between the results from the two approaches.

VI. DISCUSSION

The results of this experiment can be grouped into two classes: (a) tests of the applicability of the impulse approximation to radiative processes, and (b) the measurement of n-p bremsstrahlung. The former category includes the analysis of the events from quasifree-$pp\gamma$ and from quasifree-pn radiative capture. The observed reduction factors in the quasifree over the free radiative processes are comparable to those observed for non-radiative quasifree N-N scattering.[17,29] In the nonradiative case, impulse-approximation calculations which include S-wave final-state interactions[29-31] account for much, but not all, of the observed reduction. The remainder might be attributed to multiple-scattering terms. The similarity of the reduction factors for radiative and nonradiative processes suggests the same explanation of the reduction factors, and it implies that at the level of our accuracy the deuteron can be considered a target of "almost-free" nucleons for purposes of studying $NN\gamma$ processes. Our theoretical model proved quite satisfactory.

Beyond its function as a test reaction, the quasifree-pn radiative-capture process can be profitably used to study phenomena related to deuteron photodisintegration; in particular, polarization phenomena can be measured much more easily in the capture reaction with

[28] R. E. Cutkosky, Phys. Rev. 103, 505 (1956).

[29] D. Spalding, A. Thomas, and E. H. Thorndike, Phys. Rev. 158, 1338 (1967); A. Thomas, Ph.D. thesis, University of Rochester, 1967 (unpublished).

[30] A. H. Cromer and E. H. Thorndike, Phys. Rev. 131, 1680 (1963).

[31] C. N. Brown (private communication).

a polarized proton beam than would be possible in photodisintegration.

The n-p-bremsstrahlung result $\sigma_{np\gamma}=35\pm12$ μb is to be compared with our previous result of $\sigma_{pp\gamma}=0.70$ ±0.15 μb, giving a ratio $\sigma_{np\gamma}/\sigma_{pp\gamma}=50\pm20$, in sharp contrast to a recent theoretical prediction that the two cross sections are of comparable magnitude.[32] We also exceed by an order of magnitude the early calculation by Ashkin and Marshak,[6] who found $\sigma_{np\gamma}=2.8$ μb at an incident energy of 250 MeV. The large discrepancy could derive from the fact that neither of these treatments took account of final-state interactions between the neutron-proton pair. A study by Cutkosky[28] has shown that they will strongly enhance the cross section at the upper end of the continuous γ spectrum, in addition to forming the line spectrum corresponding to the formation of bound-state deuterons. Interpolation of Cutkosky's results at incident energies of 90 and 400 MeV gives $\sigma_{np\gamma}=22$ μb at our energy. ($E_\gamma\geqslant40$ MeV, but exclusive of the contribution from deuteron formation.) Although the linear interpolation procedure may be questionable, this result agrees rather well with our measurement. In addition, Cutkosky found that the cross section for the formation of the bound deuteron was always smaller than the $np\gamma$ cross section integrated over the upper 60% of the continuous γ spectrum. We found this ratio to be near 0.3, and it seems more plausible that the probability for the formation of the bound state is less than that for all unbound final states.

The only experimental results suitable for comparison are those of Edgington and Rose,[18] who performed a D_2O-H_2O subtraction experiment with 140-MeV incident protons. By detecting only the γ rays and measuring their energy spectrum in a lead-glass Čerenkov counter of poor energy resolution, they determined the total cross section for the production of photons of energy $E_\gamma\geqslant40$ MeV from the p-d interaction to be 4.6 ± 0.3 μb. Their spectra show very little evidence of a pn radiative-capture peak near $E_\gamma=70$ MeV, placing an upper limit of 0.10 on K_3. This contrasts sharply with our value of $K_3=0.75\pm0.10$ at 197 MeV. In order to investigate the energy dependence of K_3, we took some data[33] on the quasifree-pn radiative-capture reaction with our beam energy degraded to 146 ± 9 MeV. We found $K_3=0.68\pm0.16$ at $\theta_{\gamma c}=105°$,

which agreed well with our result at the higher energy. We must conclude that this discrepancy casts doubt on the accuracy of the Harwell results, although we are unable to pinpoint the source of the error. Edgington and Rose have interpreted their observed photon-production cross section in terms of free $np\gamma$ and arrived at the result $\sigma_{np\gamma}=8$ μb ($E_\gamma\geqslant40$ MeV). Their method of interpretation was comparable to that which gave us our upper limit of $\sigma_{np\gamma}=47$ μb. The difference cannot be explained by the difference in incident energy, if the observed energy dependence of $\sigma_{pp\gamma}$ is any guide. Hence the two experiments are also incompatible with respect to the continuous portion of the γ spectrum from n-p bremsstrahlung.

It is very difficult to perform an informative comparison between the present results and those of previous experiments which inferred $\sigma_{np\gamma}$ from the scattering of protons from complex nuclei. This is due to the wide variety of incident energies, targets, scattering angles, and detectors which have been used. Edgington and Rose[15] have given a detailed discussion of their results with targets of heavy nuclei in relation to the work of Wilson,[13] Cohen et al.,[14] and Beckham.[16] It appears that the Harwell results are larger than all others by a factor ranging from 2 to 3.5. We have taken some data concerning the γ-production cross section in the scattering of 146-MeV protons from targets made of C, Al, and Cu.[33] Our results are higher than those found at Harwell by a factor near 5, although the relative cross sections for those three complex nuclei agree rather well. Although measurements with heavy nuclei do not lend themselves to reliable interpretations in terms of n-p bremsstrahlung, such a large body of conflicting data should not remain unresolved by a careful study.

More data on n-p bremsstrahlung are needed to resolve the present discrepancy. Our large value for $\sigma_{np\gamma}$ would make a measurement of the free-$np\gamma$ process, using a neutron beam, decidedly more feasible than was previously believed. If deuterium is used as a target for a proton beam, care should be taken to keep detection thresholds to a minimum, so that the ($pd\gamma$) final state can be observed over a larger portion of phase space than was possible in this experiment. The interpretation of $\sigma_{pd\gamma}$ in terms of $\sigma_{np\gamma}$ could then be made much more reliable.

ACKNOWLEDGMENT

[32] W. A. Pearce and I. Duck, in Proceedings of the International Conference on Nucleon-Nucleon Interaction, Gainesville, Fla., 1967 (unpublished).

[33] These measurements are described in detail by P.F.M. Koehler, Ph.D. thesis, University of Rochester, 1967, Appendix C (unpublished).